

Movers and shakers: Granular damping in microgravity

M. N. Bannerman, J. E. Kollmer, A. Sack, M. Heckel, P. Mueller, and T. Pöschel

Institute for Multiscale Simulation, Universität Erlangen-Nürnberg, Nägelsbachstraße 49b, DE-91052 Erlangen, Germany

(Received 8 October 2010; revised manuscript received 18 April 2011; published 6 July 2011)

The response of an oscillating granular damper to an initial perturbation is studied using experiments performed in microgravity and granular dynamics simulations. High-speed video and image processing techniques are used to extract experimental data. An inelastic hard sphere model is developed to perform simulations and the results are in excellent agreement with the experiments. In line with previous work, a linear decay of the amplitude is observed. Although this behavior is typical for a friction-damped oscillator, through simulation it is shown that this effect is still present even when friction forces are absent. A simple expression is developed which predicts the optimal damping conditions for a given amplitude and is independent of the oscillation frequency and particle inelasticities.

DOI: [10.1103/PhysRevE.84.011301](https://doi.org/10.1103/PhysRevE.84.011301)

PACS number(s): 45.70.-n, 46.40.Ff

I. INTRODUCTION

The characteristic property of dynamic granular systems, when compared to other many-particle systems, is their ability to dissipate mechanical energy through particle collisions. While the dissipative properties of vibrated granulate have long been investigated [1,2], recently a large body of literature [3–8] has emerged on the mechanics and technical application of this damping mechanism in the form of *granular dampers*. A granular damper is a container partly filled by granular particles which may be attached to vibrating machinery to attenuate the amplitude of the oscillations. In its regime of operation, the granular material is in a gaseous state and its dynamics is determined primarily by the interparticle collisions rather than by long-lasting sliding contacts between the grains. *Static granular dampers* (e.g., Refs. [9,10]) which exploit the rheology of granular matter and *impact dampers* (e.g., Refs. [11–14]), where only one particle is located in a cavity and dissipate energy in collisions with the walls of the container, are not considered here.

Granular dampers have a number of properties which are desirable in a wide range of technical applications: Unlike traditional dampers, granular dampers do not require an anchor in order to restrict the motion of the system. This is advantageous for damping in portable equipment and in space applications where no fixed anchor is available. Granular dampers are extremely simple devices consisting solely of particles enclosed in a container or cavity and require very little maintenance. Granular dampers do not suffer from significant aging when compared to the oil and rubber components of traditional dampers. Finally, granular dampers can operate over a wide range of temperatures without performance degradation as the mechanics of the particle-particle and particle-wall interactions exhibit only a weak dependence on the temperature. Modern technical applications of granular dampers include the damping of blade integrated disks (blisks) for compressors [15], structural vibration damping [16–18], noise reduction of bank note processing machines [19], and others. Perhaps the most common application is the *dead-blow hammer* [20] as well as other impact damping handles [21].

The macroscopic damping properties of granular dampers under dynamic load is complicated, highly nonlinear, and there is no straightforward way to optimize their performance for

a given situation. This has been demonstrated in a number of experiments and molecular dynamics (MD) simulations, including investigations on the attenuation of a free spring or cantilever with an attached granular damper [5,7,22–24]. The response of an oscillating cantilever with respect to periodic forcing has also been studied [25–30]. Even more complex systems have been investigated, such as the oscillation modes of a plate with an abundance of granulate filled cavities [31–34] with the aim of noise reduction [19]. For simple systems, such as cantilever oscillators, some progress has been made. Theoretical models have been developed based on phenomenological descriptions of the multiphase gas-particle flow of granular matter for attenuating oscillations [35] and also for driven steady state oscillations [36].

A granular damper, which is a dynamical system of dissipative interacting particles, obviously must be able to dissipate energy; however, its general behavior is not clear *a priori*. Properties, such as the dissipation rate, are complex functions of the frequency and amplitude of the oscillation, as well as the particle properties, the extension and characteristics of the container or cavities, and the filling fractions. More work is needed in this field to generate experimental results and corresponding models capable of describing the dynamics of granular dampers.

Salueña *et al.* [1] have shown that several regimes of energy dissipation exist for a granular damper and that the transitions between these regimes are determined primarily by the influence of gravity. An efficient operation of a granular damper which is lightweight and needs no fixed anchor can only be expected if the average kinetic energy of the particles is much larger than their average potential energy (the damper operates in the *dynamic* or *collisional* regime). In order to carefully investigate this regime, the influence of gravity should be minimized and experimental investigations should be performed under conditions of weightlessness.

The objective of this paper is to develop an effective model for the energy dissipation of a granular damper operating in the collisional regime. Our approach is as follows: First, experiments in microgravity are performed and the attenuation of a spring with an attached granular damper for several sets of parameters is obtained (Sec. II). A model capable of reproducing the experimental results is also developed and

high-precision discrete element method (DEM) simulations are performed (Sec. III). The two free parameters of the model (coefficients of restitution) are obtained by adjusting the values until the simulation matches the experiment as closely as possible for a single experiment (Sec. III C). From the excellent agreement of the simulation results for the fitted system and *for all other* experiments, it is concluded that the model underlying the simulation replicates the system’s essential features (Sec. III D). Thus, the DEM simulations are an effective model for granular damping in the collisional regime. In Sec. IV, a simple equation for the optimal design of a simple damper is derived and tested against the results of the DEM simulations. Section V discusses the observed linear decay of the amplitude. Finally, in Sec. VI the conclusions of the paper are outlined.

II. EXPERIMENTAL SETUP

Figure 1 is a diagram of the experimental setup. Our granular damper comprises a container of adjustable length which is partially filled with granular material. The damper is mounted to one end of a spring-steel blade and the opposite end is clamped in a solid aluminum base plate. The spring blade is described fully in Sec. III C. The rectangular damper container is constructed from 5-mm-thick transparent polycarbonate plates. The internal dimensions of the container are 50 mm × 50 mm × L , where the length L (in the direction of the oscillation) is adjusted by altering the spacing of the end walls. The container’s net weight (without granulate) is $M = 434$ g. In this work, four different container lengths of $L = 40, 65, 85,$ and 104 mm are used. The damper is loaded with $N = 37$ precision steel ball bearings of diameter $\sigma = 10$ mm and mass $m = 4.04$ g. This number of particles is chosen as it packs to form a layer two particles deep on the end walls of the container.

The motion of the damper and contained granulate is recorded using a high-speed camera (MotionScope M3™),

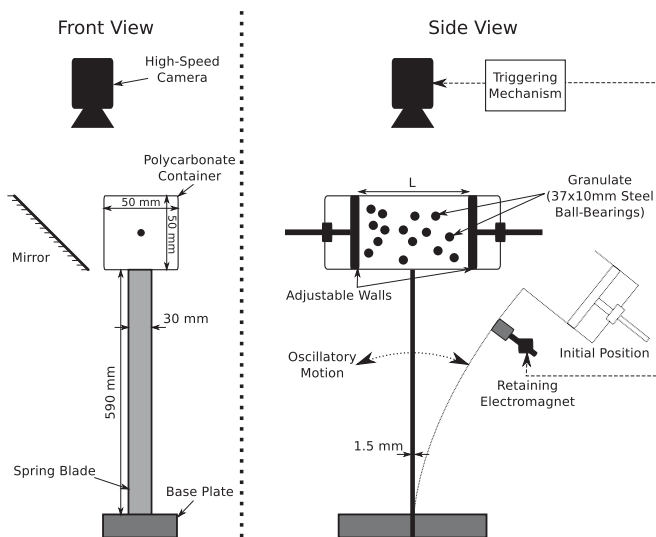


FIG. 1. Schematic of the experimental setup in front view (left) and side view (right). The curvature of the oscillations is exaggerated for the purpose of illustration.



FIG. 2. An example frame from the high-speed camera. An example video which compares simulation and experimental results is available online [37].

which records at a frame rate of 500 fps and with a spatial resolution of 1024×1280 pixels. A 45° mirror is placed at the side of the container and allows for the simultaneous observation of the granulate from the top and the side (see Fig. 2). The position of the damper and the center of gravity of the particles are extracted from the top view using standard image-processing techniques. Although the side view facilitates more complex methods of reconstruction, it will be shown that the motion of the granulate is well described by the center of mass motion. All position measurements are made in a two-dimensional (2D) plane which is parallel to and intersecting the top of the container while it is in its equilibrium position. Although this introduces some error at the peaks of the oscillations due to the curved damper trajectory, this error is negligible.

At the start of the experiment, the spring blade is deflected and held at the initial displacement of $\Delta_0 = 107.5$ mm using an electromagnet. A trigger mechanism begins the experiment and starts the camera recording. After a short delay of 1 s, the spring blade is released from the electromagnet and the oscillations are recorded for 30 s.

To assure conditions of weightlessness, the experiment is performed on a modified Airbus A300 aircraft which has been retrofitted for performing parabolic flights. The parabolic flight provides a suitable microgravity environment (± 0.05 g) which lasts around 22 s and allows a number of experiments to be performed. In the following section, the numerical model and simulation techniques are described.

III. NUMERICAL MODEL AND SIMULATION METHOD

A sufficiently complex model, capable of reproducing the observed experimental behavior, must be found if the system’s dynamics is to be understood. The model presented here is complex enough to yield quantitative agreement with the experiments and yet simple enough to gain insight into the dynamics of the system. The model for the granulate consists of a system of $N = 37$ smooth inelastic hard spheres, each of mass $m = 4.04$ g and diameter $\sigma = 10$ mm. Although inelastic hard spheres are a basic model for the granulate they capture all of the essential behavior of the system: dissipative interactions between hard spherical particles.

To model the oscillating mass and granular damper, the hard spheres are shaken in a rectangular box of mass M , which is coupled to a linear spring. The box is assumed

to remain parallel to the axis of the system and oscillate along only one axis. By only permitting oscillations in a single dimension, this model neglects the arcing motion of the blade spring (see Fig. 1) and oscillatory modes induced by the collisions of the particles with the box. However, these effects are expected to be small in comparison to the dynamics of the modeled oscillation. With these approximations, the collision-free motion of the box can then be modeled using a simple harmonic oscillator

$$\vec{r}_{\text{box}}(t) = \hat{n} \Delta \cos[2\pi\omega(t + t_{\text{shift}})] + \vec{r}_{\text{box}}^{(0)}, \quad (1)$$

where \vec{r}_{box} is the current position of the oscillator, $\vec{r}_{\text{box}}^{(0)}$ is its equilibrium position, \hat{n} is the unit vector in the direction of the oscillation, and ω is the frequency of the empty damper. The amplitude of the oscillation Δ and the phase shift of the oscillator t_{shift} are dynamical quantities and are altered by particle-box interactions. At time $t = 0$, the plate is at its positive maximum ($t_{\text{shift}} = 0$) with an initial displacement of $\Delta = \Delta_0$.

The methods for performing event-driven simulations using smooth hard spheres and fixed walls are well established (e.g., see Ref. [38]) and will not be discussed in detail. Here an event-driven dynamics simulation package (DynamO [39]) is used to simulate the dynamics of granular-damped oscillators. The only extension to the basic event-driven method concerns the detection and execution of events between particles and the oscillating boundary walls perpendicular to the oscillation direction \hat{n} , which is discussed in the following sections.

A. Detecting oscillating wall interactions

Event-driven algorithms require an expression to calculate if and when a collision (an *event*) occurs between a particle and the bounding walls of the damper. If a collision is detected and it is the next event to occur in the system, the system is moved to the time of the collision and the event is executed by updating the velocities of the colliding particle, and the phase shift t_{shift} and amplitude Δ of the oscillator.

To determine the time at which a particle i will collide with an oscillating wall, the equations of motion for the particle and the oscillating plate must be solved. Essentially, this is a search for the shortest positive root Δt of the function

$$f(\Delta t) = [\vec{r}_i + \Delta t \vec{v}_i - \vec{r}_{\text{box}}(\Delta t + t)] \cdot \hat{n} \pm \left(\frac{L - \sigma}{2} \right) = 0, \quad (2)$$

where \vec{r}_i and \vec{v}_i are the position and velocity of particle i at the current system time t , and Δt is the time until collision. The sign of the term $\pm(L - \sigma)/2$ is used to set which side of the oscillating box is tested for collisions.

To guarantee that no roots are missed, the root finding technique of Frenkel and Maguire [40] is used. This root finding routine requires a fixed interval to search for possible roots. The upper bound on the interval to search is determined from the time the freely moving particle takes to cross the extrema of the tested wall's oscillation,

$$\Delta t_{\text{max}} = \frac{\text{sgn}(\hat{n} \cdot \vec{v}_i)([L - \sigma]/2 + \Delta) - \hat{n} \cdot (\vec{r}_i - \vec{r}_{\text{box}}^{(0)})}{\hat{n} \cdot \vec{v}_i}, \quad (3)$$

where $\text{sgn}(x)$ is the sign function. The lower bound is typically the current system time ($\Delta t_{\text{min}} = 0$). However, if the last event to occur was a collision between this particle and an oscillating wall, the lower bound is increased to avoid redetecting the same root. The lower bound is then set to

$$\Delta t_{\text{min}} = \frac{|2\dot{f}(0)|}{\ddot{f}_{\text{max}}}, \quad (4)$$

where $\ddot{f}_{\text{max}} = \Delta \omega^2$ is the maximum absolute second derivative of Eq. (2). The root finding technique used to search for suitable roots of Eq. (2) iterates towards a root from the boundaries of the interval by approximating the function at each iteration with a parabola. The equation of the parabola is generated using the derivatives of Eq. (2) and its smallest root provides the next iteration point. The iterations are halted on the n th iteration once the following criterion is met:

$$|\Delta t_n - \Delta t_{n-1}| < \frac{[L - \sigma]}{2\ddot{f}_{\text{max}}} \times 10^{-12}, \quad (5)$$

where $\dot{f}_{\text{max}} = |\vec{v}_i \cdot \hat{n}| + 2\pi\omega\Delta$ is the maximum absolute first derivative of Eq. (2). Unlike the hard line system of Frenkel and Maguire [40], all roots of Eq. (2) are acceptable and only the earliest root must be found. This completes the description of the collision detection and root finding technique.

B. Executing particle-oscillating wall collisions

The final part of the simulation algorithm concerns the execution of oscillating boundary wall collisions. The conservation of momentum and the assumption of a constant coefficient of restitution leads to

$$\Delta \vec{p}_i = -\Delta \vec{p}_{\text{wall}} = -\frac{mM(1 + \varepsilon_{\text{pw}})}{m + M}(\hat{n} \cdot [\vec{v}_i - \dot{\vec{r}}_{\text{box}}])\hat{n}, \quad (6)$$

where $\Delta \vec{p}_i$ and $\Delta \vec{p}_{\text{wall}}$ are the momentum change of the colliding particle i and oscillating wall, respectively, and ε_{pw} is the coefficient of restitution for particle-wall collisions. During a collision, the phase t_{shift} and amplitude Δ of the oscillating wall are altered under the constraints of conserving momentum and the current box position. This results in the following expressions for the postcollision state of the oscillating plate:

$$t'_{\text{shift}} = \frac{1}{\omega} \arctan \left(\frac{-\hat{n} \cdot [\Delta \vec{p}_{\text{box}} + \dot{\vec{r}}_{\text{box}}]}{2\pi\omega\hat{n} \cdot [\vec{r}_{\text{box}} - \vec{r}_{\text{box}}^{(0)}]} \right) - t, \quad (7)$$

$$\Delta' = \frac{\hat{n} \cdot (\vec{r}_{\text{box}} - \vec{r}_{\text{box}}^{(0)})}{\cos(2\pi\omega[t + t'_{\text{shift}}])}, \quad (8)$$

where the primes denote postcollision values. Care must be taken at this point in the calculation to ensure that the magnitudes of t and t_{shift} do not affect the precision of the calculations. Care must also be taken to retain the correct quadrant of the calculated angle when using the arctan function (e.g., by using the C function $a \tan 2$).

A difficulty with the event-driven simulation method arises from its inability to simulate events with finite durations. When the oscillating wall is accelerating, a particle can repeatedly collide with the plate until its relative velocity and separation are numerically zero. Physically, the particle sticks to the wall and is pushed until the plate enters the deceleration phase of its oscillation or interacts with another particle. To prevent this

TABLE I. Model parameters for the event-driven simulations.

σ (mm)	m (g)	N	Δ_0 (mm)	ω (s ⁻¹)	M (g)	ε_{pp}	ε_{pw}
10	4.04	37	107.5	1.23	434	0.75	0.76

unresolvable situation from occurring within the event-driven simulation, the interactions between the oscillating wall and a particle are turned elastic when

$$\frac{\hat{n} \cdot (\vec{v}_i - \dot{\vec{r}}_{\text{box}})}{\pi \omega \Delta} < 0.04. \quad (9)$$

The pushing of the particle is then transformed into a sequence of small hops which, as in the physical pushed case, do not dissipate energy. As this expression is linear in the current displacement Δ , the long time behavior of the system is still recovered ($\Delta \rightarrow 0$ as $t \rightarrow \infty$). This elastic approximation is small when the plate motion dominates the dynamics of the system and the results appear to be unaffected if smaller values for Eq. (9) are used.

C. Parameters of the simulation

The simulations are initialized with all particles arranged in a regular lattice (fcc), with initial velocities assigned from a Gaussian and a total particle energy less than $<0.002\%$ of the initial spring energy. The particles are packed in a loose layer on the wall at the initial extrema of the oscillation. The particles in the experiment are also typically arranged this way due to the influence of gravity before the microgravity phase of the experiment.

The simulations require several inputs and these parameters are reported in Table I. All parameters, with the exception of the box frequency ω and coefficients of restitution ε_{pp} and ε_{pw} , are directly obtained from the experimental setup described in Sec. II. The three remaining parameters must be calculated from material parameters or obtained through experimental results.

The frequency of the unloaded damper ω may be estimated using the simple harmonic oscillator model. The spring constant of the spring blade may be calculated using the Euler-Bernoulli beam equation

$$k = \frac{Ewh^3}{4l^3} = 25.4 \text{ N m}^{-1}, \quad (10)$$

where $E = 2.06 \times 10^{11} \text{ N m}^{-2}$ is the elastic modulus of the spring steel, $w = 30 \text{ mm}$ is the spring width, $h = 1.5 \text{ mm}$ is the spring thickness, and $l = 590 \text{ mm}$ is the spring length. If the system behaves as a simple harmonic oscillator and the mass of the spring is ignored, the frequency may be estimated using

$$\omega \approx \frac{1}{2\pi} \sqrt{\frac{k}{M}} \approx 1.217 \text{ s}^{-1}. \quad (11)$$

The frequency of the loaded granular damper ω_{system} is lower than that of the empty damper ω due to the added mass and the interactions of the granulate. In the simple harmonic oscillator

model, the additional mass of the granulate alters the frequency of the oscillations by

$$\omega_{\text{loaded}} = \omega \sqrt{\frac{M}{M + Nm}}. \quad (12)$$

In the limit that the granulate is tightly packed in the granular damper, the frequency of the system should limit to the simple harmonic oscillator frequency $\omega_{\text{system}} \rightarrow \omega_{\text{loaded}}$. In the limit of a large box, the granulate will completely decouple from the oscillator and $\omega_{\text{system}} \rightarrow \omega$. Remarkably, the frequency of the experimental oscillators, obtained through averaging the peak and center point frequencies, is consistent for all box lengths at approximately $\omega_{\text{system}} \approx 1.05 \text{ s}^{-1}$ with a standard deviation of $\pm 0.01 \text{ s}^{-1}$. If it is assumed that $\omega_{\text{system}} \approx \omega_{\text{loaded}}$ for small box lengths, Eq. (12) estimates an unloaded frequency of $\omega \approx 1.22 \pm 0.1 \text{ s}^{-1}$ for the experimental system. This agreement with the beam equation is promising and suggests that, although the granulate is periodically decoupled from the oscillator, the deviation from Eq. (12) is still small for the experimental box lengths studied here. For the simulations, a slightly higher frequency of $\omega \approx 1.23 \text{ s}^{-1}$ is used which is within the standard deviation of the experimental values and yields an excellent fit to the experimental data.

Finally, the coefficients of restitution ε_{pp} and ε_{pw} describing the inelastic collisions between particles and between a particle and the wall must be determined. These model parameters are obtained by fitting simulation results to the experimental data for the smallest box length ($L = 40 \text{ mm}$, Fig. 3). As best fits the following results are obtained:

$$\varepsilon_{pp} = 0.75, \quad \varepsilon_{pw} = 0.76. \quad (13)$$

The value for the particle-wall coefficient of restitution is in close agreement with published results reported for a 9.35 mm steel ball bearing impacting a clamped acrylic plate [41]. However, the particle-particle coefficient of restitution is significantly lower than expected. Performing an automated drop test [42] of the granulate on to a silicon carbide plate yields a coefficient of restitution of $\varepsilon \approx 0.95$. Due to the high rigidity of the base plate, this value should be close to the experimental value for particle-particle interactions. The fitted particle-particle coefficient of restitution ε_{pp} may be unexpectedly lower than the drop test results due to missing dissipation mechanisms in the model (e.g., granulate friction). Despite this, the agreement of the simulation and experimental results (see Sec. III D) shows that this is still an effective model for the system.

It should be noted that the fitting of the coefficients of restitution ε_{pp} and ε_{pw} is performed exclusively for the box width of $L = 40 \text{ mm}$. For all other simulations reported here, the optimized coefficients of restitution are used without further fitting.

D. Validation of the numerical method

The simulation and experimental results are compared in this section to validate the model. Figure 3 presents the box position x_{box} and the granulate center of mass x_{COM} as a function of time for a box length of $L = 40 \text{ mm}$. Two experimental measurements are reported and both are in close agreement with the simulation results. The experimental and simulation

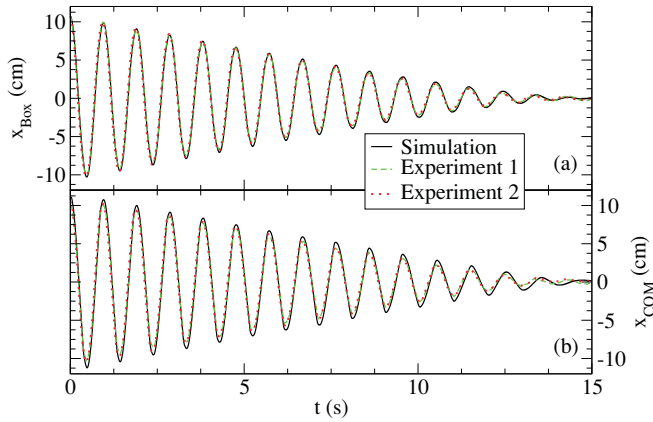


FIG. 3. (Color online) A comparison of simulation results and experimental data for (a) the box position x_{box} and (b) the granulate center of mass x_{COM} as a function of time for a box length of $L = 40$ mm. The simulation data is fitted to the experimental data through the coefficients of restitution $\varepsilon_{\text{pp}} = 0.75$ and $\varepsilon_{\text{pw}} = 0.76$.

results display a high degree of repeatability (compare Figs. 3 and 4) and single realizations are representative of the averaged values. This is due to the uniqueness of the initial state, with the spring held in a deflected state and the particles resting in a regular, repeatable layer on the outer wall due to the influence of gravity before the microgravity phase. However, the experimental results begin to fluctuate toward the end of the microgravity phase due to disturbances in the flight.

The numerical result for the box position x_{box} as a function of time is in excellent quantitative agreement with the experimental data. For the position of the center of mass x_{COM} the agreement is also very good albeit not as close as for $x_{\text{box}}(t)$, with some overestimations near the peaks of the oscillations. The error could arise from the experimental method due to the top-down view of the simulation and 2D image reconstruction used. The area of the visible particles is identified and the centroid location is taken to be the center of mass. Due to the end walls and slight arcing motion of the box (see Fig. 1)

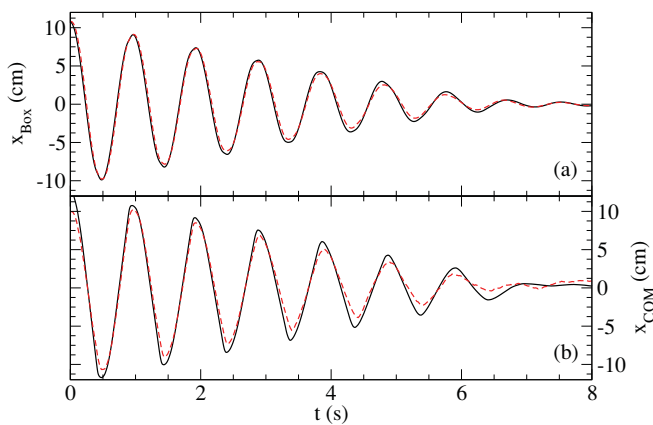


FIG. 4. (Color online) A comparison of simulation results and experimental data for (a) the box position x_{box} and (b) the granulate center of mass x_{COM} as a function of time for a second experiment at the box length of $L = 40$ mm. Line types are described in Fig. 3. The simulation data is not fitted to this data set and the parameters of Fig. 3 are used.

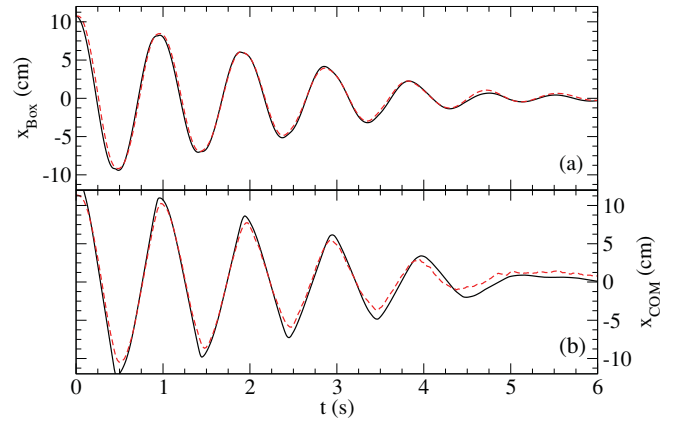


FIG. 5. (Color online) The same comparison as Fig. 4, but for a box length of $L = 85$ mm. Note the change of time scale.

the reconstructed center of mass is slightly biased toward the center of the box.

The agreement between the simulation and experiment for the frequency of the damped oscillator is excellent and confirms the accuracy of the fundamental frequency ω . However, the excellent agreement in the amplitudes between experimental data and simulations for $L = 40$ mm is perhaps not too surprising since this experimental data set is used to determine the coefficients of restitution, ε_{pp} and ε_{pw} . The model parameters are now fixed and the numerical result for several different box widths are compared with the corresponding experimental data (see Figs. 4–6).

In general, the simulation results are in excellent agreement with the model's predictions. This implies that the approximations of the model (one-dimensional oscillations, no air resistance, ideal spring) are small and have little effect on the dynamics of the granular damper. Some of these approximations may already be compensated for in the fitting of the coefficients of restitution, but they appear to be well behaved with the changes in box length. In the simulation, rotational degrees of freedom are neglected by eliminating friction between the particles, and between a particle and the container walls. In contrast to vibrated granular dampers in gravity (where the energy dissipation due to friction is of the same scale as energy dissipation by impact [43]), in

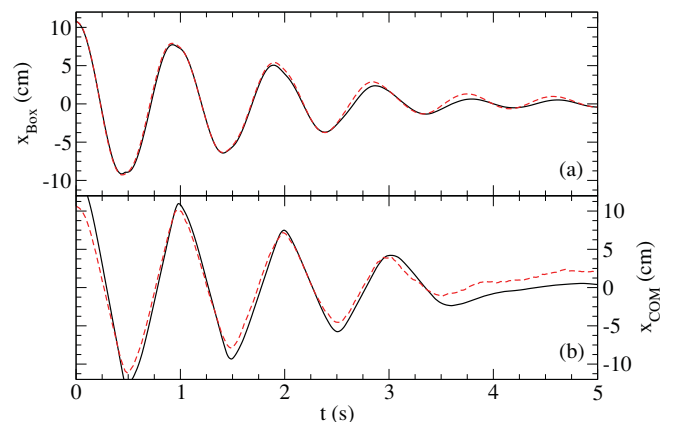


FIG. 6. (Color online) The same comparison as Fig. 4, but for a box length of $L = 104$ mm. Note the change of time scale.

microgravity, friction seems to be less important or easily characterized into the restitution coefficient ε_{pp} . Overall, the fitting of the coefficients of restitution appears to be effective at capturing the behavior of the system and no further parameters or extensions of the simulation model are required.

The most striking feature of the curves in Figs. 3–6 is the linear decay of the peak amplitude of the oscillation with time. A detailed discussion of this property is postponed to Sec. V and optimal dampers are discussed in the following section.

IV. OPTIMAL DAMPERS

There is a significant dependence of the damping efficiency on the container length, as is seen in Figs. 3–6. The number of cycles before the oscillations are sufficiently damped varies from 13 to 4 as the box length is increased. By examining the energy transfer mechanisms within the granular damper, an expression for optimizing the damper's design may be found.

Figure 7 plots the cumulative energy lost through the three classes of collisions in the simulation system. It should be noted that Fig. 7 is only valid for the fitted coefficients of restitution and will therefore differ from the true experimental values. Nevertheless, the results should agree qualitatively and allow some insight into the experimental system. The sides of the box appear to be unimportant in this design of a damper and may present an opportunity for optimization by utilizing alternative shaker geometries (e.g., an hourglass design). Although the inclusion of friction forces in the simulation will increase the sidewall dissipation, the video observations of the granulate show little or no drag on the cluster during the flying phase. This indicates that these friction forces are relatively small as the granulate is densely packed and in contact with the wall (see Fig. 2) but shows no effect from sliding against the wall.

Not only are the particle–end-wall collisions the sole mechanism for the transferral of oscillation energy from the oscillator into the contained granulate, but simulation results estimate that these collisions are also a significant dissipation mechanism for the damper. The end-wall interactions both transfer and dissipate the maximum energy when the relative velocity of the oscillator end walls and granulate are maximized. Therefore, maximizing this relative speed should optimize the performance of the granular damper. In the following section, an attempt is made to estimate the optimal box length using a simple model for the dynamics.

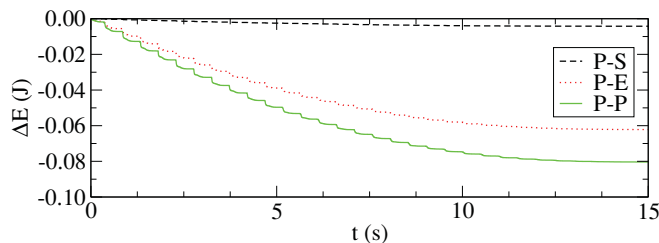


FIG. 7. (Color online) Simulation values for the cumulative energy loss through interactions with the side walls (P-S), end walls (P-E) and particle-particle interactions (P-P) for a box length of $L = 40$ mm.

A. Theoretical predictions

Attempting to optimize the system by modeling the granulate as a single particle or some other simplified description is difficult [44] due to the lack of an analytical solution to Eq. (2). To estimate the optimal damping conditions, only two plausible assumptions for the motion of the granulate in the box are required: (a) the granulate will be “collected” and form a packed layer on the approaching oscillating wall during the initial inward stroke (when the oscillator accelerates towards the center point), and (b) the center of mass velocity of the granulate at the end of the inward stroke is, on average, the maximum oscillator velocity. The time from the center of the stroke at which the granulate would hit the peak displacement of the oscillator is then given by

$$t_{g,\text{peak}} = \frac{L + \Delta - \sigma_{\text{layer}}}{2\pi\omega_{\text{loaded}}\Delta}, \quad (14)$$

where $\sigma_{\text{layer}} = 2\sigma = 20$ mm is the thickness of the layer of granulate when it is packed on the surface of the oscillating wall. This is a good estimate of the layer thickness as the particles are smooth, monodisperse, and the number was selected to ensure that they do not jam easily in an irregular packing (see Fig. 2 and Ref. [37]). It should be noted that Eq. (14) decreases in time, as Δ decreases on average due to interactions with the granulate. If for any integer n the peak collision time lies in the range $n < \omega t_{g,\text{peak}} < n + \frac{1}{4}$, the granulate will hit the oscillating wall on the outward phase of its stroke. All experimental boxes with the exception of the largest system ($L = 104$ mm) are within this regime. It is expected that improved damping occurs if the granulate hits on the inward stroke as the relative velocity is maximized.

The granulate travels the length of the box in

$$t_{g,\text{box}} = \frac{L - \sigma_{\text{layer}}}{2\pi\omega_{\text{loaded}}\Delta}. \quad (15)$$

If $n + \frac{1}{4} > \omega t_{g,\text{peak}} > n + 1$ and $n < \omega t_{g,\text{box}} < n + \frac{1}{2}$, the granulate will collide on the inward phase of the stroke. The largest system, where $\omega t_{g,\text{box}} \approx 0.15$, collides after the turning point of the oscillator. However, the dissipation is maximized when $\omega t_{g,\text{box}} \approx \frac{1}{2}$. At this point, the relative velocity between the granulate and oscillating box is also maximized. For $\omega t_{g,\text{box}} > \frac{1}{2}$ the plate is either decelerating or multiple cycles of the oscillation occur without the granulate colliding.

The damping of the oscillator from the initial state can be optimized, independently of the coefficients of restitution, by altering either L , ω , or Δ such that $\omega t_{g,\text{box}} \approx \frac{1}{2}$. Efficiency will be lost and recovered as Δ changes over time, but if the granulate is relatively inelastic this will occur after most of the energy is dissipated or transferred in the first cycle.

Setting $\omega t_{g,\text{box}} = \frac{1}{2}$ in Eq. (15) and using Eq. (12), the optimal box length L_{opt} may be estimated for a given initial amplitude Δ_0 using

$$L_{\text{opt}} = \pi\Delta_0\sqrt{\frac{M}{M + Nm}} + \sigma_{\text{layer}}. \quad (16)$$

This expression is remarkable in that it is independent of the oscillation frequency. This may be understood from dimensional analysis as, due to the negligible initial kinetic energy, the model has only one time scale. As such, the

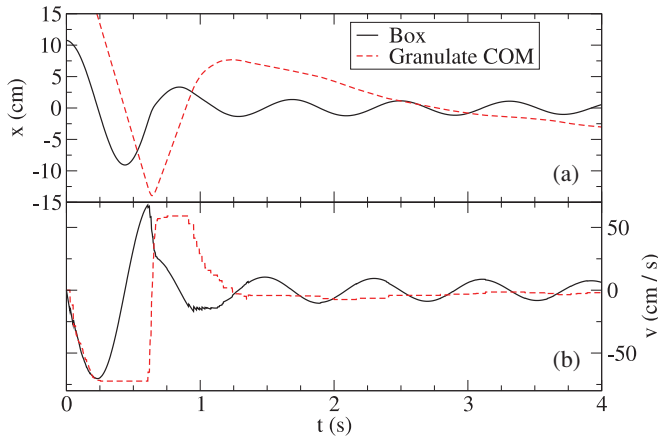


FIG. 8. (Color online) A comparison of simulation results and experimental data for the box and granulate (a) position, and (b) velocity as a function of time for the optimal box length of $L = 311$ mm, as predicted by Eq. (16). Note the change of time scale.

solutions to the model must scale trivially in the frequency of the oscillations. In the following section, the results of Eq. (16) and its assumptions are checked against simulation results.

B. Numerical test

The validity of the basic assumptions made in Sec. IV A and the result, Eq. (16), are now tested using the results of the DEM simulations. Using Eq. (16) to predict the optimal box length for the damping of the experimental system yields a value of $L_{\text{opt}} = 311$ mm. The results of a simulation at this box length are presented in Fig. 8. A square step in the granulate center of mass velocity is visible at the peak of the box velocity as the granulate decouples from the oscillator. The assumption of an equal box and granulate velocity at the midpoint of the stroke (at peak velocity) appears to hold. Visual inspection [37] confirms the granulate is collected in a layer on the approaching oscillating wall. The recollision of the granulate also appears to occur close to the peak of the box velocity, maximizing the relative velocity, energy dissipation, and energy transfer in this first collision. The largest oscillations are effectively damped within one second. However, the oscillator is now susceptible to smaller amplitude oscillations which appear to decay very slowly. The optimal approach would be to couple two or more dampers to damp a wider range of amplitudes within short time scales. This idea has already been pursued for impact dampers (e.g., Ref. [45]) which are related to granular dampers except that in the container or cavity there is only a single particle.

To test the predictions of Eq. (16) for the optimal damping length L , a suitable metric must be defined to compare various box lengths. Figure 9 compares the time an oscillator takes to dissipate a certain fraction of the initial energy as a function of the box length. Despite the continuing low-amplitude oscillations of the damper at $L = 311$ mm (see Fig. 8), the damper effectively eliminates 95% of the initial energy in well under two oscillations. Equation (16) appears to yield an excellent estimate for the global optimal box length, avoiding both the highly inefficient zones toward the edges of the graph. Previous work on forced granular dampers (e.g., see Fig. 7

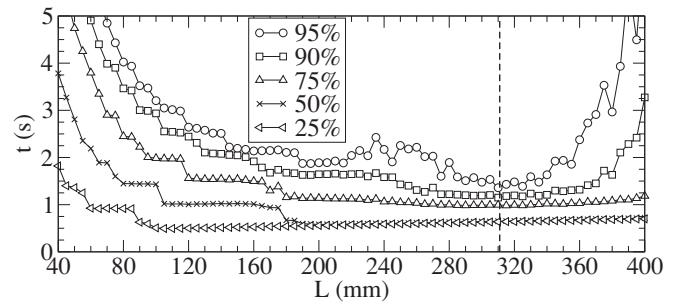


FIG. 9. Simulation results for the time t to dissipate a percentage of the initial energy, versus the box length L . The vertical dashed line indicates the optimal box length as predicted by Eq. (16).

in Ref. [25]) also yields performance curves with the same general U shape as Fig. 9.

V. LINEAR DECAY

Figures 3–6 reveal a linear decay of the amplitude of the oscillation with time, and thus the energy of the system decays quadratically in time. This is highlighted in Fig. 10, where the time dependence of the square root of the total energy of the damper is plotted. This behavior is a common motif in granular dampers and has been reported previously [3,7,23,24,46,47], even for single-particle dampers. Surprisingly, the same behavior is also found for rather different dampers such as thrust-based damping [48] and impact dampers [49–52]. However, this is not a general rule and other published results exist (e.g., Ref. [5]) where a nonlinear decay of the amplitude of the oscillation (possibly exponential) is found. The result is surprising as the common viscous dampers yield an exponential decay of the amplitude. The linear decay of a static granular damper may be due to the frictional forces in the system; however, the simulations carried out in this paper reproduce the linear decay in the absence of frictional or viscoelastic interactions. This is in contrast to previous simulation or experimental studies.

This result is also surprising if the approximations of the previous section are used to perform dimensional analysis. To recap, the oscillator appears to have a constant frequency for a given box length, and the oscillator collects the granulate on a wall and then collides the granulate in each half period. For the amplitude decay to be linear, the energy dissipated in each of these “collisions” of the granulate must then be proportional to the amplitude Δ . However, if an inelastic particle with a constant coefficient of restitution is given a

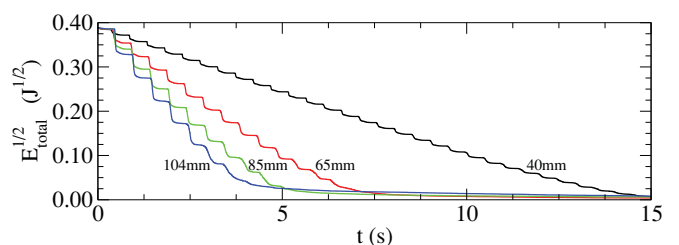


FIG. 10. (Color online) Total energies of the oscillators as obtained from numerical simulations.

velocity proportional to the maximum plate velocity ($2\pi\omega\Delta$), it will dissipate energy proportional to the square of the plate amplitude (Δ^2) for any nonzero number of collisions. Therefore, despite the simplicity of the current model, no simple explanation is yet available for the linear decay and further research is required to explore this effect.

VI. CONCLUSIONS

In this paper, a method for performing controlled experiments on granular damped oscillators in microgravity is outlined. High-speed video capture and image-processing techniques are used to reconstruct the motion of the oscillator to obtain accurate experimental results. A simple hard sphere model and event-driven dynamics are also used to generate quantitative results that compare well against the experimental values. From the excellent agreement of the simulation and experimental frequency, it appears that the damper frequency responds like a simple harmonic oscillator to changes in load [Eq. (12)] for short box lengths. This is remarkable given the periodic decoupling of the granulate from the spring and box. The simulation model scales trivially with the frequency of the oscillations as, apart from the negligible initial energy, the model has only one time scale. Further research is required on experimental systems to determine the frequency dependence of granular dampers and generalize the current model to these systems. This may require extending the current model to a velocity dependent coefficient of restitution.

The model has two major limitations which must be discussed. First, friction forces are absent in the model. These forces are typically vital to capture granular dynamics and are dominant in quasistatic regimes. However, it is shown here that by the excellent agreement with the experiment that the frictional forces are effectively approximated by the coefficient of restitution and/or the frictional effects are small in this system. Another limitation is that the particle model contains no inherent time scale. Therefore, the model has only a trivial dependence on the frequency of the oscillations. The granular dampers here operate in a “collect and collide” regime and with microgravity conditions and the high Young’s modulus of steel (200 GPa) it is not expected that there is a strong dependency on the frequency. Despite these limitations, the

model has several advantages. The model is computationally cheap when compared to Hertz models of systems with a high Young’s modulus. The model is also simple enough to allow theoretical analysis (see Sec. IV) and is used here to explore the significance of frictional effects in granular dampers.

The straightforward design of these granular dampers yields a remarkably simple expression for the optimal damping configuration of the form of Eq. (16). Simulations at the predicted optimal box length damp large-amplitude oscillations remarkably well (see Fig. 8) but are susceptible to smaller-amplitude disturbances. The final expression for the optimal box length is independent of the oscillation frequency, due to the lack of a time scale in the simulation and theoretical model.

Unlike conventional viscous-damped systems, the granular damped system studied here displays a linear decay in the amplitude. This behavior is not intuitive and is a feature typical of friction-damped oscillators. This work clarifies that this apparent frictional behavior may also arise solely from the collisional granular dynamics and does not necessarily arise from friction or viscoelastic forces within the experimental setup. The linear decay is a useful property as it implies that a granular damper can completely damp oscillations within a finite time. However, this is not the case as, at low oscillation energies a transition occurs and the damping force is significantly reduced. Further research is required in designing dampers with a wider amplitude response by coupling multiple dampers with different lengths. The internal geometries may also be optimized to eliminate the decoupling of the granulate in the midpoint of the stroke to create more effective dampers.

ACKNOWLEDGMENTS

The authors would like to acknowledge the German Science Foundation (DFG) for funding via Grant No. FOR608 and the DLR for funding the parabolic flight campaign. Thanks also go to the mechanical workshop NW2 at the University of Bayreuth and Knut Reinhardt for advice regarding the mechanical setup. Finally, the authors would like to acknowledge the additional funding of the DFG through the Cluster of Excellence Engineering of Advanced Materials in Erlangen.

-
- [1] C. Salueña, T. Pöschel, and S. E. Esipov, *Phys. Rev. E* **59**, 4422 (1999).
 - [2] C. Salueña, S. E. Esipov, T. Pöschel, and S. Simonian, *Proc. SPIE* **3327**, 23 (1998).
 - [3] K. Mao, M. Wang, Z. Xu, and T. Chen, *J. Vib. Acoust.* **126**, 202 (2004).
 - [4] K. Mao, Z. Xu, M. Wang, and T. Chen, in *Proc. IMPLAST* (2003), pp. 994–1005.
 - [5] K. Mao, M. Y. Wang, Z. Xu, and T. Chen, *Powder Technol.* **142**, 154 (2004).
 - [6] C. Tianning, K. Mao, H. Xieqing, and M. Wang, *Proc. SPIE* **4331**, 294 (2001).
 - [7] X.-M. Bai, L. M. Keer, Q. J. Wang, and R. Q. Snurr, *Granular Matter* **11**, 417 (2009).
 - [8] X.-M. Bai, B. Shah, L. M. Keer, Q. J. Wang, and R. Q. Snurr, *Powder Technol.* **189**, 115 (2008).
 - [9] J. Bourinet and D. Houédec, *Comput. Struct.* **73**, 395 (1999).
 - [10] K. Cowden, D. Bishop, D. Walrath, and J. McInroy, *Proc. SPIE* **5052**, 317 (2003).
 - [11] C. Cempel, *J. Sound Vib.* **40**, 249 (1975).
 - [12] S. F. Masri, *J. Acoust. Soc. Am.* **47**, 229 (1970).
 - [13] S. F. Masri, *J. Acoust. Soc. Am.* **45**, 1111 (1969).
 - [14] M. Duncan, C. Wassgren, and C. Krousgrill, *J. Sound Vib.* **286**, 123 (2005).
 - [15] R. Kielb, F. G. Macri, D. Oeth, A. D. Nashi, P. Macioce, H. Panossian, and F. Lieghley, *Proceedings of the National Turbine Engine High Cycle Fatigue Conf.* (1999).
 - [16] H. V. Panossian, *J. Vib. Acoust.* **114**, 101 (1992).

- [17] C. Cempel and G. Lotz, *J. Struct. Eng.* **119**, 2624 (1993).
- [18] J. R. Fricke, *S.V. Sound Vib.* **34**, 22 (2000).
- [19] Z. W. Xu, M. Y. Wang, and T. N. Chen, *J. Sound Vib.* **270**, 1033 (2004).
- [20] J. C. Norcross, Dead-Blow Hammer Head, U.S. Patent No. 3343576 (1967).
- [21] S. Ashley, *Mech. Eng. (Am. Soc. Mech. Eng.)* **117**, 80 (1995).
- [22] V. Kinra, K. Marhadi, and B. Witt, *46th AIAA/ASME/ASCE/AHS/ASC Structures, Structural Dynamics, and Materials Conference* (2005), Vol. 9, p. 6376.
- [23] K. S. Marhadi, Master's thesis, Texas A&M University, 2003.
- [24] R. Friend and V. Kinra, *J. Sound Vib.* **233**, 93 (2000).
- [25] M. Saeki, *J. Sound Vib.* **251**, 153 (2002).
- [26] M. Saeki, *J. Sound Vib.* **281**, 1133 (2005).
- [27] B. Fowler, E. Flint, and S. Olson, *Proc. SPIE* **3989**, 356 (2000).
- [28] B. L. Fowler, E. M. Flint, and S. E. Olsen, *Proc. SPIE* **4331**, 186 (2001).
- [29] A. Papalou and S. Masri, *J. Vibr. Control* **4**, 361 (1998).
- [30] C. X. Wong, M. C. Daniel, and J. A. Rongong, *J. Sound Vib.* **319**, 91 (2009).
- [31] Z. W. Xu, M. Y. Wang, and T. N. Chen, *J. Vib. Acoust.* **126**, 141 (2004).
- [32] Z. W. Xu, M. Y. Wang, and T. N. Chen, *J. Sound Vib.* **279**, 1097 (2005).
- [33] J. Park and D. L. Palumbo, *Exp. Mech.* **49**, 697 (2009).
- [34] B. L. Fowler, Air Force Research Laboratory Technical Report No. A771024, 2003.
- [35] C. Wu, W. Liao, and M. Wang, *J. Vib. Acoust.* **126**, 196 (2004).
- [36] X. Fang and J. Tang, *J. Vib. Acoust.* **128**, 489 (2006).
- [37] See Supplemental Material at <http://link.aps.org/supplemental/10.1103/PhysRevE.84.011301> for a slow-motion (16×) video comparing the simulation and experiment for a box length of $L = 40$ mm.
- [38] T. Pöschel and T. Schwager, *Computational Granular Dynamics* (Springer, New York, 2005).
- [39] M. Bannerman, R. Sargant, and L. Lue (submitted to *J. Comp. Chem.*), e-print [arXiv:1004.3501v1](https://arxiv.org/abs/1004.3501v1).
- [40] D. Frenkel and J. F. Maguire, *Mol. Phys.* **49**, 503 (1983).
- [41] R. Sondergaard, K. Chaney, and C. E. Brennen, *J. Appl. Mech.* **57**, 694 (1990).
- [42] M. Montaine, M. Heckel, C. Kruelle, T. Schwager, and T. Pöschel (unpublished), e-print [arXiv:1104.0049v1](https://arxiv.org/abs/1104.0049v1) [cond-mat.stat-mech].
- [43] T. Chen, K. Mao, X. Huang, and M. Y. Wang, *Proc. SPIE* **4331**, 294 (2001).
- [44] N. Popplewell and M. Liao, *J. Sound Vib.* **146**, 519 (1991).
- [45] S. F. Masri, *J. Acoust. Soc. Am.* **45**, 1111 (1969).
- [46] K. S. Marhadi and V. K. Kinra, *J. Sound Vib.* **283**, 433 (2005).
- [47] S. Ekwaro-Osire and I. C. Desen, *J. Vib. Control* **7**, 475 (2001).
- [48] B. M. Shah, D. Pillet, X.-M. Bai, L. M. Keer, Q. J. Wang, and R. Q. Snurr, *J. Sound Vib.* **326**, 489 (2009).
- [49] W. M. Mansour and D. R. T. Filho, *J. Sound Vib.* **33**, 247 (1974).
- [50] M. Y. Yang, G. H. Koopmann, G. A. Lesieutre, and S. A. Hambric, *ASME Conference Proceedings* (2002), p. 113.
- [51] C. C. Cheng and J. Y. Wang, *Int. J. Mech. Sci.* **45**, 589 (2003).
- [52] Y. Du, S. Wang, Y. Zhu, L. Li, and G. Han, *Adv. Acoust. Vibr.* **2008**, 140894 (2008).